Design and Control of a Magnetically-Actuated Anti-Interference Microrobot for Targeted Therapeutic Delivery

Yanding Qin, *Member, IEEE*, Zhuocong Cai, and Jianda Han, *Member, IEEE*

***Abstract*—This paper proposes an anti-interference targeted therapeutic delivery microrobot, where the targeted therapeutic delivery to the lesion site in human intestine can be operated by the external magnetic field. The robot is composed of a shell and a targeted delivery mechanism. Under the actuation of the external magnetic field, the spiral structure on the outer surface of the shell can actively moves the robot back and forth in human intestine. The internal embedded targeted delivery mechanism is fixed with a radial magnetized O-type permanent magnet. It not only realizes flexible movement in the fluid environment, but also realizes the intestinal anchoring and targeted therapeutic delivery functions against the constant peristalsis of human intestine. The proposed robot is designed to finish the drug treatment concentration and treatment effect precisely in the lesion site against the intestinal peristalsis. A series of simulations and experiments are conducted to evaluate the feasibility of the developed robot. In experiments, the robot is used to release drugs after anchoring in the lesion site. Finally, ex vivo experiments are carried out on fresh porcine intestines.**

***Index Terms*—Magnetic actuation microrobot, targeted therapeutic delivery, anti-interference, intestinal anchoring.**

I. Introduction

MICROROBOT has widely attracted attention for its great potential in biomedical field, which has brought historic progress to the examination and treatment of human gastrointestinal tract [1-3]. Great research efforts have been directed towards the active motion control and path planning of the microrobot, and there are many breakthrough research advances [4-6]. However, the treatment function cannot fully satisfy the clinical requirements. When a certain intestinal disease needs drug treatment, invasive treatment such as endoscopy will cause trauma to the patient. Meanwhile, oral drugs can easily reach the lesion site at insufficient concentration due to the influence of gastric acid or intestinal mucus, reducing the treatment effect [7-11]. Therefore, how to enable microrobot to achieve targeted therapy to the lesion site in the constantly peristaltic intestinal tract has become a research hotspot [12-15].

In order to solve this problem, many researchers have investigated the drug delivery function using microrobot. Pi et al. developed a new type of solid propellant micro thruster [16]. The structure generates energy through the chemical reaction in the micro thruster and sends a signal through the external device to trigger the drug delivery. Dietzel et al. proposed an active agent release system consisting of two magnets as drug container [17]. When reaching the lesion site, the magnets can be separated by the external magnetic field to release the drug. Beccani et al. proposed a magnetic drug delivery capsule with embedded coil [18]. When the external signal is triggered, the coil is activated, and a repulsive force is generated between the two magnets, resulting in the release of drugs.

However, if only large-scale and large-dose administration is considered, microrobot cannot accurately move to the lesion site, and cannot achieve targeted administration in human intestine. Moreover, the normal tissues will also be injured. Therefore, how to accurately navigate and target the lesion site has been widely investigated [19-23]. Le et al. proposed a passive drug delivery device based on the remote control of soft magnets [24]. The robot is driven to the lesion site by an external magnetic field, and a suitable magnetic field is applied to demagnetize the magnet. The two soft magnets lose magnetism and release the drugs in the capsule. Cai et al. developed a magnetically controlled targeted drug delivery microrobot, which can actively move to the lesion site [25]. The microrobot has a cam structure connected with a radial magnetized permanent magnet. The cam rotates through the rotating magnetic field to realize the targeted drug delivery function. Wang et al. proposed a new magnetically driven multi-module microrobot for drug sustained-release [26]. The internal propeller realized active motion, and the drug cabinet pushed the drugs out like a syringe, realizing the sustained-release and quantitative drug delivery. However, although the robot can accurately move to the lesion site to release drugs, it cannot stay at the lesion site due to the peristalsis of human intestinal tract. Thus, it cannot ensure that the released drugs are applied to the lesion site. In this case, the drug concentration might be too low and the treatment effect will be affected [27-29].

Due to the constant peristalsis of human intestine, it is crucial for most intestinal diseases to receive sustained medication at the lesion site. In this paper, an anti-interference targeted therapeutic delivery microrobot (ATTDM) is proposed, which is remotely operated by an external permanent magnet (EPM) to deliver the treatment to the lesion site of the peristaltic human intestine. Furthermore, an internal embedded targeted delivery mechanism is fixed with radial magnetized O-type internal permanent magnet (IPM), which realizes flexible movement in the fluid environment.

The contribution of the proposed ATTDM can be summarized as follows:

(1) ATTDM is equipped with targeted delivery mechanism to easily achieve targeted drug delivery at the capsule scale.

(2) ATTDM can not only actively move to the lesion site via external magnetic field control, but also anchor in the constantly peristaltic intestine for targeted drug delivery.

This work was supported in part by the Natural Science Foundation of Tianjin under Grant 18JCZDJC39100, and in part by the National Natural Science Foundation of China under Grant 52005270. *(Corresponding author: Jianda Han.)*

All the authors are with the College of Artificial Intelligence, Nankai University, Tianjin 300350, China, and also with the Institute of Intelligence Technology and Robotic Systems, Shenzhen Research Institute of Nankai University, Shenzhen 518083, China (e-mails: qinyd@nankai.edu.cn; caizhuocong@hotmail.com; hanjianda@nankai.edu.cn).

(3) ATTDM provides an enabling method for targeted therapeutic delivery against the intestinal peristalsis.

II. Concept and Design

Fig. 1(a) shows the concept of the clinical scenario of ATTDM in human intestinal tract. The system is divided into the primary control system and the secondary processing system. ATTDM at the secondary end, controlled by the primary controller, realizes the intestinal targeted therapeutic delivery function. The detailed clinical process is described as follows. First, the patient drinks a certain amount of water after cleaning the intestine to provide conditions for the active movement of ATTDM. Second, the patient swallows ATTDM under the guidance of the doctor and lies in the diagnosis and treatment area of the secondary processing system. Next, the doctor runs the magnetic actuation system through the primary console to control the motion mode of ATTDM. When reaching the lesion site, ATTDM is switched to targeted therapeutic delivery mode, and it anchors in the constantly peristaltic intestine and applies drugs to the lesion site, as shown in Fig. 1(b). After the diagnosis and treatment functions are completed, ATTDM switch back to motion mode and will be discharged through the digestive system.

A. Structure Design of ATTDM

The model of ATTDM is shown in Fig. 1(c). The spiral structure can generate propulsion force when rotating in a fluid environment. Compared with the driving structures of various capsule robots [30], the spiral structure has the best motion characteristics in the fluid environment and is designed as the power supply of the robot. The explosive structure of ATTDM is shown in Fig. 1(d). When ATTDM is moving, the internal part is shown in Fig. 1(e). Through the magnetic dipole moment generated by EPM and IPM, the movement direction and rotation velocity of ATTDM are controlled so that it can accurately reach the lesion site. The interior of ATTDM during targeted application is shown in Fig. 1(f), where the rotating EPM generates a rotating magnetic field to rotate IPM and the targeted delivery mechanism. As a result, anchoring arms are pushed out and anchored in the constantly peristaltic intestine to overcome interference and release drugs. At the end of the targeted therapeutic delivery, the magnetic field is controlled to restore ATTDM to the motion mode and continue to move. By changing the rotation direction and velocity of the EPM, ATTDM can be controlled to move freely in various environments, and anti-interference anchoring and targeted application therapy can be performed in the lesion site.

As shown in Fig. 1(d), the ATTDM consists of a spiral structure, a bearing, a targeted delivery mechanism, four anchoring arms, an IPM (material: NdFeB35), and a fixed rod. The targeted delivery mechanism and IPM are fixed, and IPM is magnetized in the vertical direction. When IPM rotates axially, ATTDM can rotate, move, and switch the motion mode. When IPM rotates radially, the targeted delivery mechanism, driven by IPM, performs the anchoring task and delivers the drug treatment in a targeted manner.

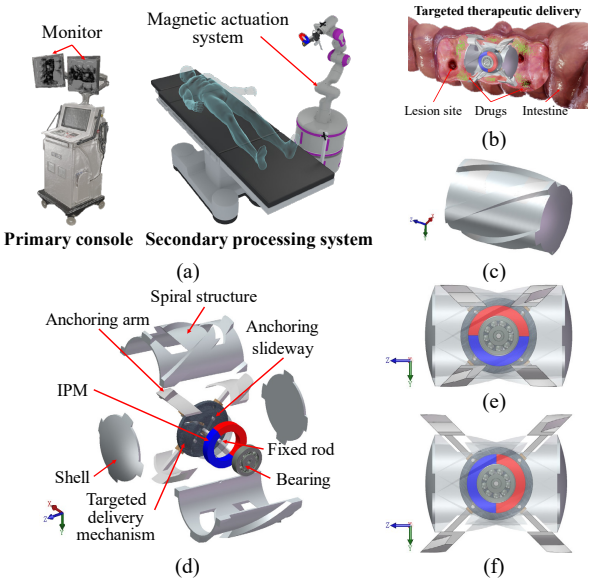

Fig. 1. (a) Schematic diagram of ATTDM system, (b) Principle of targeted therapeutic delivery using ATTDM, (c) and (d) The isometric and explosive views of ATTDM, (e) and (f) Sectional views of ATTDM in motion and targeted therapeutic delivery modes.

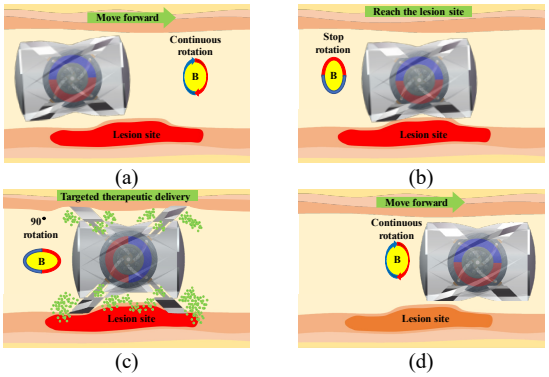

Fig. 2. Working principle of ATTDM: (a) move forward, (b) reach the lesion site, (c) targeted therapeutic delivery, (d) move forward.

B. Working Principle of ATTDM

The working principle of ATTDM is shown in Fig. 2. When the patient swallows ATTDM to the initial position of the intestine, it is ready to start the examination and treatment of the intestine, as shown in Fig. 2(a). In the fluid filled intestinal environment, the IPM embedded in ATTDM keeps synchronous rotation axially by the rotation of the EPM, and ATTDM will move forward relying on the fluid reaction force generated by the rotation of the spiral structure, as shown in Fig. 2(b). When ATTDM reaches the lesion site, IPM rotates radially to expand the targeted delivery mechanism. The targeted delivery mechanism pushes anchoring arms, so that ATTDM can be fixed in the constantly peristaltic intestine, enter the targeted therapeutic delivery mode, and release drugs. During this period, ATTDM can prevent insufficient drug concentration caused by intestinal peristalsis or robot passive movement to non-pathological areas, as shown in Fig. 2(c). After the treatment is completed, change the direction of the magnetic field to restore it to the motion mode, as shown in Fig. 2(d). Subsequently, ATTDM continues to move and is finally discharged from the body.

III. Control Strategy

According to Newton's second law of motion, the motion behavior of ATTDM in fluid is analyzed, and the distribution of capsule machine manpower is simplified, including the propulsion force F_p, the resistance force F_r, the magnetic force F_m, the buoyancy force F_b and the gravity force F_g. Their relationship is expressed as [30]:

$$m\frac{\partial v}{\partial t} = F_p - F_r + F_m \sin\theta_f \pm F_b \sin\theta_f \mp F_g \sin\theta_f \quad (1)$$

where m is the mass of ATTDM, θ_f is the included angle between ATTDM and the standard horizontal plane. Based on the theory of fluid mechanics, when ATTDM moves in the fluid environment, the volume of liquid passing through any vertical plane in any time interval is the same at any position. The cross-sectional areas A_1 and A_2 are the fluid inflow area and outflow area of ATTDM, respectively. The volume of liquid flowing into ATTDM per unit time is equal to the volume of liquid flowing out, which can be expressed as:

$$Q = S_1 v_1 = S_2 v_2 \quad (2)$$

where Q is the liquid flow through the spiral structure, v_1 is the inflow velocity of the inflow area S_1, and v_2 is the outflow velocity of the outflow area S_2.

The resistance force of ATTDM can be expressed as [30]:

$$F_r = \tfrac{1}{2} C_d \rho S_1 v_1^2 + \mu_f F_n \quad (3)$$

where C_d is the resistance coefficient, ρ is the liquid density, μ_f is the friction coefficient, and F_n is the normal force between ATTDM and the human intestinal surface.

Therefore, the propulsion force F_p of ATTDM can be expressed as:

$$F_p = \rho A_2 v_2^2 - \tfrac{1}{2} C_D \rho S_1 v_1^2 - \mu_f F_n \quad (4)$$

A. Magnetic Actuation Principle

The EPM is used as the driver to control the IPM and ATTDM, which can realize flexible adjustment of the space position and orientation [31]. EPM is fixed to the flange of a robot and rotated by a motor. It can easily generate a uniform rotating magnetic field with arbitrary rotating velocity in any direction in an open large-scale space.

However, if the distance between ATTDM and EPM is too large, the magnetic flux density applied to ATTDM will be too small to drive its movement. On the contrary, the excessive magnetic force will cause ATTDM and EPM to attract each other, which may injure the intestinal tract [32]. Thus, keeping proper distance between ATTDM and EPM is a key factor for accurate control of ATTDM.

As shown in Fig. 3, when the magnetic torque T_M is equal to the maximum circumferential friction torque T_f, there is a maximum control distance $d_{\max}$. At this time, the driving torque of ATTDM is 0 Nm and it cannot rotate. When the magnetic force F_m is equal to the gravity force F_g, there is a minimum control distance $d_{\min}$. ATTDM will be attracted to the intestine and cannot move. It can be expressed as:

$$\begin{cases} d_{\max} : T_m = T_f \\ d_{\min} : F_m = F_g \end{cases} \quad (5)$$

When the change in magnetic force enables ATTDM to eliminate the interference of gravity and buoyancy in the horizontal direction, ATTDM achieves the optimal control distance [32]. According to the magnetic coupling theory, the coupling magnetic torque of the universal rotating magnetic vector acting on the permanent magnet is perpendicular to the plane formed by the magnetic moment vector and the magnetic vector of the permanent magnet. Then the external magnetic field will generate the torque driving the robot, that is, a torque of T_m is generated between EPM and IPM:

$$T_m = B m_r \sin\theta_m \quad (6)$$

where m_r is the magnetic moment vector of the permanent magnet and B is the magnetic vector of the rotating magnetic field, θ_m is the slip angle between the rotating magnetic field vector and the magnetic moment vector of the permanent magnet embedded in ATTDM.

B. Dynamics Modeling

Based on the hydrodynamics theory, the dynamic modeling of ATTDM is established, as shown in Fig. 3. For the convenience of analysis, the coordinate axis is built in Fig. 3, where u_c and v_a are defined as the circumferential and axial velocities, respectively, U and W are the velocity projections of u_c and v_a along and perpendicular to the helical direction, respectively, and θ is the angle of microrobot spiral. Then U and W can be combined by u_c and v_a [30]:

$$\begin{bmatrix} W \\ U \end{bmatrix} = \begin{bmatrix} \cos\theta & -\sin\theta \\ \sin\theta & \cos\theta \end{bmatrix} \begin{bmatrix} v_a \\ u_c \end{bmatrix} \quad (7)$$

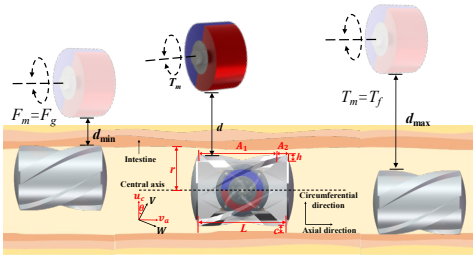

Fig. 3. Magnetic actuation principle of ATTDM.

According to the Reynolds equation, $p_1(x)$ and $p_2(x)$ are the pressure distributions at A_1 and A_2, respectively, which are obtained as follows:

$$\begin{bmatrix} p_1(x) \\ p_2(x) \end{bmatrix} = \begin{bmatrix} \frac{6\mu\gamma(1-\beta)}{G(1+\gamma)^2} & 0 & 0 \\ 0 & \frac{6a\mu\beta\gamma(1+\gamma)^2}{G} & -\frac{x}{G} \end{bmatrix} \begin{bmatrix} W_1^2 x \\ W_2^2 \\ W_2^2 x \end{bmatrix} \quad (8)$$

where $\alpha = A_1 + A_2$, $\beta = A_2/\alpha$, $\gamma = h/c$, $G = c^2[(1-\beta)\, W_1 + \beta(1+\gamma)\, W_2]$, L is the length of the spiral structure, c is the distance between the thread and the intestine, h is the height of the thread, and μ is the fluid viscosity.

According to Navier-Stokes equations, the theory of hydrodynamic lubrication and Newton's law of internal friction, the shear stress of ATTDM under the action of fluid can be expressed as:

$$\begin{cases} F_x = \int\int \left(-\mu \frac{h}{2} \frac{\partial^2 W}{\partial z^2} - \frac{\mu W}{h} \right) \mathrm{d}y\mathrm{d}x \\ F_y = \int\int \left(-\mu \frac{h}{2} \frac{\partial^2 U}{\partial z^2} - \frac{\mu U}{h} \right) \mathrm{d}y\mathrm{d}x \end{cases} \quad (9)$$

Therefore, when the spiral structure of ATTDM rotates, the axial propulsive force and radical circumferential friction

resistance are expressed as:

$$\begin{cases} F_p = F_y \sin\theta - F_x \cos\theta \\ F_r = F_y \cos\theta + F_x \sin\theta \end{cases} \tag{10}$$

The circumferential friction torque T_f can be expressed as:

$$T_f = F_r \cdot r \tag{11}$$

C. Anchoring Modeling

As shown in Fig. 4(a), when ATTDM moves to the lesion site, anchoring arms are pushed out by rotating the targeted delivery mechanism via the rotation of the EPM. The anchor structure is accurately anchored in the intestinal tract and resists the interference of intestinal peristalsis to perform the drug delivery treatment. As shown in Fig. 4(b), the pushing out distance of the anchor structure r_v can be expressed as:

$$r_v = \sqrt{2}\theta_E (d_1 - d_2)/\pi \tag{12}$$

where θ_E represents the rotation angle of EPM, and the maximum pushing out distance is $(d_1\text{-}d_2)/\sqrt{2}$ in the vertical direction.

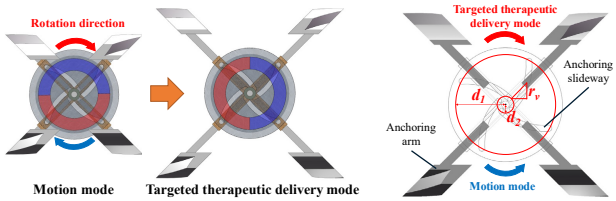

Fig. 4. (a) Anchoring process. (b) Anchoring modeling.

IV. Hydrodynamic Modeling and Analysis

Hydrodynamic characteristics are the key indexes of the robot in fluid environment. Each structural parameter has different effects on the hydrodynamic characteristics of ATTDM. Experimental testing using 3D printed prototypes is laborious and time-consuming. Therefore, in the determination of the structural parameters, finite element analysis is conducted to investigate the influence of a series of important structural parameters. In order to establish an appropriate model, some conditions need to be set. First, the central axis of ATTDM always coincides with the central axis of the intestinal tract without considering the deformation of the intestinal tract. Secondly, water is taken as the experimental fluid set in simulation and regarded as a viscous incompressible fluid. In clinics, according to surgical regulations, patients need to clean the intestine with a large amount of water before taking the capsule robot [33]. This operation fills the intestine with water, which creates a good environment for the movement of the capsule robot. Finally, since the main purpose is to investigate the influence of the structural parameters, some other forces of ATTDM, such as gravity and buoyancy, are ignored, and the motion of ATTDM is only affected by the propulsion force and resistance.

A fluid environment is established in ANSYS. In fluid simulation, the complex internal structure of ATTDM is simplified as it hardly affects the overall motion performance. A regular cylinder with a length of 425 mm and a diameter of 22 mm is used to simulate the intestinal tract. ATTDM is placed in the middle of the pipeline, and the parts not participating in the fluid simulation are removed from the flow field. Coarse meshing and fine meshing are adopted for the intestinal model and the dynamic flow field of ATTDM, respectively. Using the hexahedral mesh, the total amount of elements is maintained between 300000 and 400000 so as to guarantee the precision of analysis.

In order to obtain more accurate results in finite element analysis, the solver is set as the k-epsilon turbulence model featuring wide applicability, reliability, and convergence. The model is particularly applicable to external flow problems in regular geometry (such as the intestine) [34]. Semi-Implicit Method for Pressure-Linked Equations (SIMPLE) algorithm solves the coupling equations of pressure and velocity in simulation. In the unit area condition section, the rotation axis is set as the frame motion rotating about the Z-axis. Then, the inlet boundary is set as the pressure-inlet, the outlet boundary is set as the pressure-outlet, and the other boundary is set as the wall. Four planes without any physical significance are selected to monitor the pressure, velocity, and other parameters. Finally, select the default divergence coefficient, set the convergence standard to 0.0001, and the maximum iteration number is set to 800.

There are too many structural parameters in ATTDM. For the simplicity, only the cases with different number of threads are discussed here. All the other parameters are invariant. The robot models with 2 to 5 threads are established and analyzed. Other parameters L, θ and γ are set to be 25 mm, 35° and 0.5, respectively. The samples of velocity contour results when ATTDM moves at a rotation velocity of 15 Hz are shown in Fig. 5. The results show that when the spiral structure rotates, the fluid can pass through the inlet. The channel between the intestinal tract and the shell can effectively pressurize and discharge the fluid, so that the fluid flow rate at the outlet rises sharply.

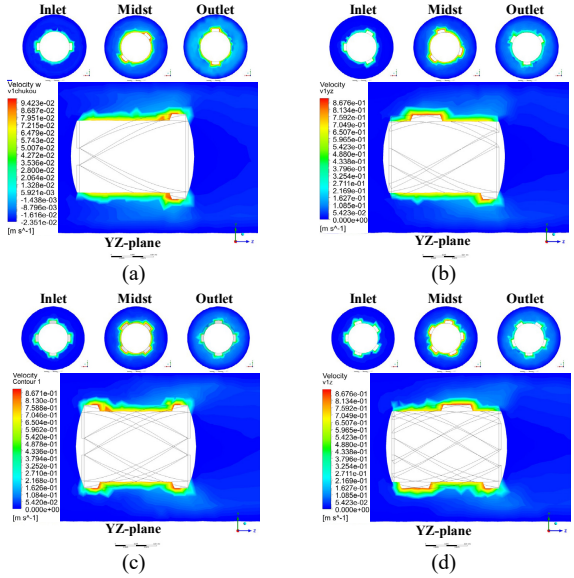

Fig. 5. Simulation results on velocity contour with different thread numbers: (a) 2-thread, (b) 3-thread, (c) 4-thread, and (d) 5-thread.

The relationship between the rotation velocity of ATTDM and the propulsion force is shown in Fig. 6. The results show that the propulsion force increases exponentially with the increase of the rotation velocity of ATTDM. Moreover, under the same rotation velocity, the motion performance of 4-thread is the best. Therefore, the structure of ATTDM is finalized using the 4-thread spiral structure.

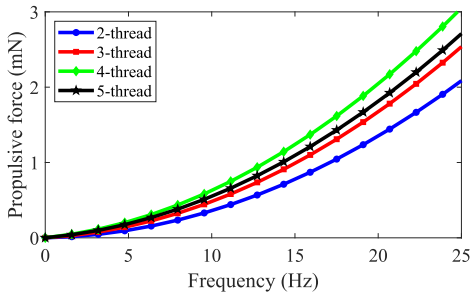

Fig. 6. Relationship between the rotation velocity of ATTDM and the propulsive force.

Subsequently, the ATTDM model in targeted therapeutic delivery mode anchored in the intestine is established, and the simulation results of velocity contour are shown in Fig. 7. The results show that when ATTDM reaches the lesion site for targeted drug treatment, with the expanding of the targeted delivery mechanism, the channel between the drug chamber and the shell can effectively pressurize and discharge the fluid drug. Therefore, the embedded fluid drug gradually flows out, and targeted drug delivery can be completed on the lesion site of the intestine.

Through simulation, some numerical values which are difficult to obtain theoretically or experimentally can be obtained. The dynamic equation of ATTDM can be simplified and optimized to accurately control the strategy of ATTDM to improve the control accuracy and motion stability.

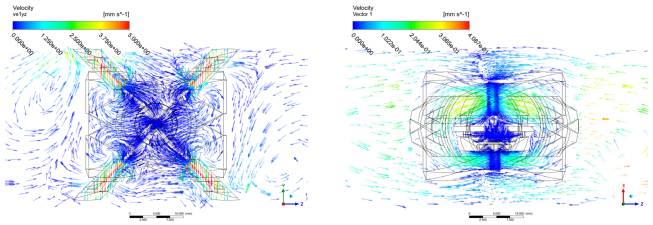

(a) (b)

Fig. 7. (a) Simulation results on axis-plane velocity contour. (b) Simulation results on bottom-plane velocity contour.

V. Experiment Results

The experimental setup is shown in Fig. 8(a). ATTDM is placed in a transparent acrylic pipe with an inner diameter of 26 mm and a length of 400 mm. The acrylic pipe is filled with water (water density: 998.203 kg/m^3) at 26°C and placed in an X-ray fluoroscopy system. The operator controls the robot arm and EPM through the PC controller, thereby controlling the position and posture of ATTDM. A peristaltic pump is used to simulate the peristaltic environment of human intestine.

Through 3D printing technology, ATTDM is fabricated using photosensitive resin to quickly test the feasibility. In the future trials in clinics, a biocompatible material, BioMed Resin from Formlabs, can be used to avoid potential risks and injury to human intestine [35]. The main structural parameters of ATTDM and permanent magnet are listed in Table I. The prototype of ATTDM is shown in Fig. 8(b). The thread pitch, height, and width of ATTDM are 2 mm, and the maximum pushing out distance of the targeted delivery mechanism in the vertical direction is 2.82 mm, as shown in Fig. 8(c). The structural design meets both process requirements and the medical dimension requirements, that is, the maximum size that can pass through the curved part of the intestine is Φ20×33.2 mm [25].

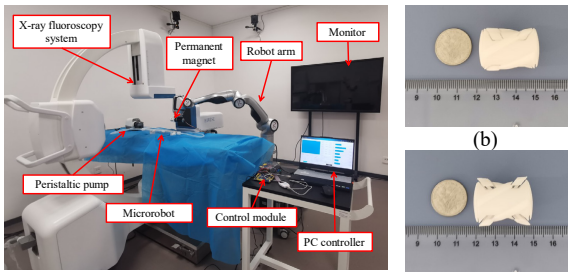

Fig. 8. (a) The experimental setup. (b) Prototypes of ATTDM. (c) Targeted therapeutic delivery mode.

TABLE I
Specifications of The ATTDM and Magnets. (Unit: mm)

Parameter	OD & ID	Length & Height
Spiral structure	20 (16)	25(2)
Shell	20 (14)	1.5(1)
Targeted delivery mechanism	6.5 (1.5)	4(4)
IPM	8 (4)	2
EPM	30	20

A. Motion Characteristics of ATTDM

The control of ATTDM is important as it needs to guarantee that EPM can remotely rotate ATTDM, and the attraction force cannot be too large to scratch the intestinal tract. Through experiments, it is found that the maximum and minimum control distances to drive ATTDM are 146 mm and 33 mm, respectively. In this range, ATTDM can be precisely controlled to perform forward, backward, and steering motion. Accordingly, the maximum and minimum control distances to anchor ATTDM are 112 mm and 20 mm, respectively. In this range, ATTDM can be precisely controlled for any degree of anchoring.

Further, the motion characteristics of ATTDM are evaluated. During the experiment, the rotation frequency of EPM is increased at an interval of 1 Hz. The control distance was set to 60 mm to obtain the relationship between the rotation frequency and the motion velocity of ATTDM. The prototype of ATTDM is placed in a 26 mm pipe filled with water. The simulation and experimental results of motion characteristics are obtained and shown in Fig. 9(a). The experimental results are obtained by averaging ten measurements, which shows that there is a linear relationship between the frequency and the motion velocity of ATTDM before 12 Hz. Due to the lack of resistance in the simulation, the simulation result is higher than the experimental results.

In addition, when the rotation frequency of EPM reaches 13 Hz, ATTDM enters the cut-off state and cannot continue to move. This is because IPM cannot keep the same frequency as EPM. Therefore, 12 Hz is set to be the cut-off frequency of ATTDM. Moreover, ATTDM has the same motion characteristics when moving backward.

The results of the motion performance of ATTDM under different intestinal diameters are shown in Fig. 9 (b), where a linear relationship can still be observed between the frequency and the motion velocity. At a control distance of 60 mm, the maximum motion velocity for pipe diameters of 22 mm, 24 mm, and 26 mm are 34.91 mm/s, 33.04 mm/s, and 32.47 mm/s, respectively. It can be concluded that changes in intestinal diameter slightly affect the motion performance of ATTDM. Furthermore, the starting frequency and cut-off frequency of ATTDM are not affected by the pipe diameter.

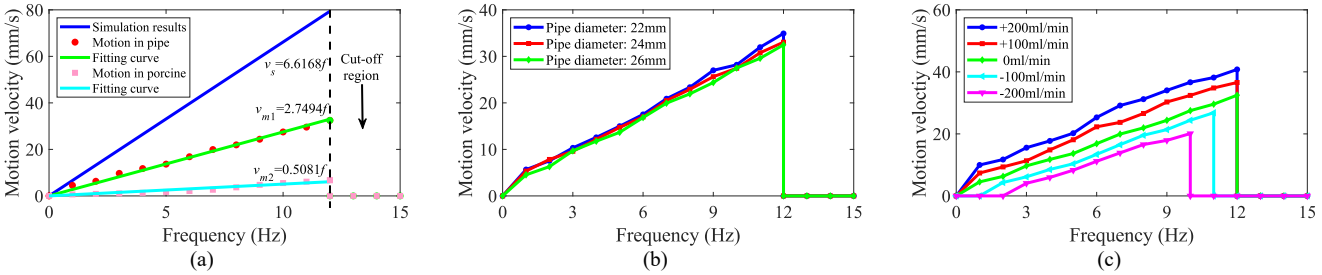

Fig. 9. (a) Relationship between frequency and motion velocity of ATTDM. (b) Motion characteristics of ATTDM at different pipe diameter environment. (c) Motion characteristics of ATTDM at different flow rate environment.

The peristalsis velocity of human intestine is random, and the maximum value can reach ±202.8 ml/min under the diameter of 26 mm [33]. Therefore, the relationship between the motion velocity and the frequency of ATTDM is obtained under the conditions that the flow rate is +200 ml/min, +100 ml/min, -100 ml/min, and -200 ml/min, respectively, as shown in Fig. 9(c). The experimental results show that there is a linear relationship between the frequency and the motion velocity when ATTDM can move normally. The maximum velocity of ATTDM in still water is 32.47 mm/s, the maximum velocity is 40.78 mm/s when the flow rate is +200 ml/min, and the maximum velocity is 13.98 mm/s when the flow rate is -200 ml/min.

Furthermore, when the flow rate is -100 ml/min and -200 ml/min, ATTDM starts to move forward at 2 Hz and 3 Hz because ATTDM cannot generate enough propulsion force to overcome the resistance of the fluid. With the increase of the circumferential friction force, the magnetic torque generated by EPM remains unchanged, which leads to the drop of the cut-off frequency of ATTDM. When the flow rate is -100 ml/min or -200 ml/min, the cut-off frequency of ATTDM drops to 11 Hz and 10 Hz, respectively. Due to the inherent properties of ATTDM, when the frequency exceeds 12 Hz, ATTDM cannot follow the rotation of EPM. Thus, even when the flow rate is +100 ml/min or +200 ml/min, the cut-off frequency of ATTDM is still 12 Hz. In addition, under the control distance of 60 mm, ATTDM could keep in place at a flow rate of -453 ml/min, exhibiting strong anti-interference capability.

B. Targeted Therapeutic Delivery of ATTDM

According to the task requirements of ATTDM in human intestine, the peristaltic pump is used to simulate the whole process of the targeted drug application task at the flow rate of -200 ml/min, as shown in Fig. 10. ATTDM is internally equipped with red granules of drugs, which can be targeted for therapeutic delivery according to the set lesion site. First, ATTDM starts to move from its initial position, as shown in Fig. 10(a). By controlling EPM, the embedded IPM rotates axially and moves forward under the action of the fluid reaction force until it reaches the lesion site, as shown in Fig. 10(b). Subsequently, EPM is controlled to make IPM rotate radially, drive the targeted delivery mechanism to push anchoring arms, and release the drug after anchoring, as shown in Fig. 10(c) and (d). At the flow rate of -200 ml/min, ATTDM releases many drugs to treat the lesion site, as shown in Fig. 10(e). Finally, ATTDM completes the targeted therapeutic delivery, and moves forward to finally expel from the pipe, as shown in Fig. 10(f). Furthermore, ATTDM can resist the maximum flow rate of -1207 ml/min in the targeted therapeutic delivery mode, which is far beyond the flow rate of the human intestine.

Fig. 11 shows the position of ATTDM during the targeted therapeutic delivery process. At 25th second, ATTDM arrived at the lesion site, and EPM used for ATTDM's motion mode is switched to the EPM for targeted therapeutic delivery mode. During the transition, under the action of the peristalsis, ATTDM is pushed backward by 13 mm. Then, EPM used for targeted therapeutic delivery mode controls ATTDM to adjust its posture and anchor, so that it can finish targeted therapeutic delivery. The whole process of targeted therapeutic delivery is 115 seconds.

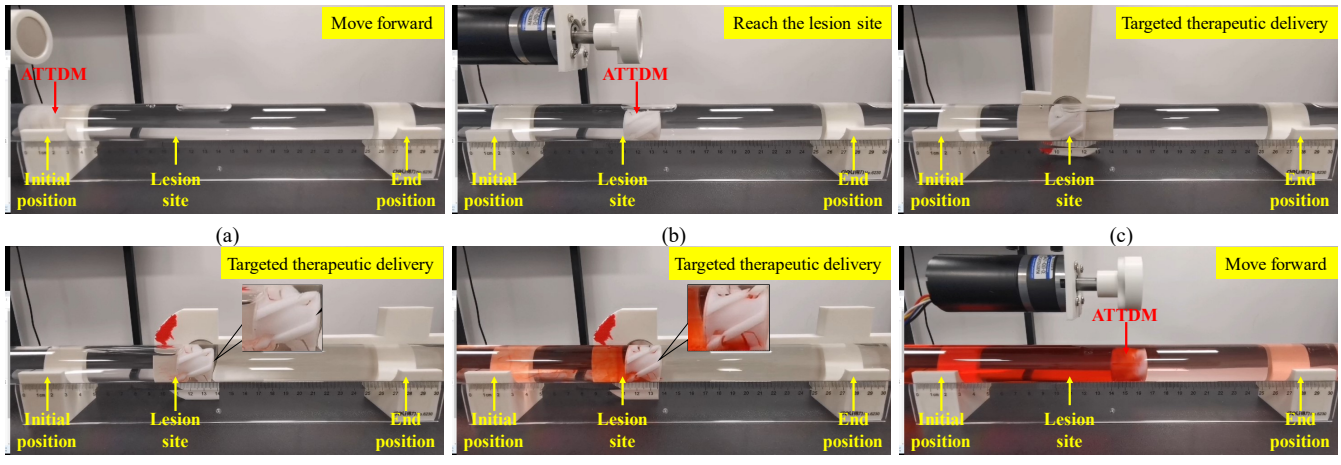

Fig. 10. (a) Start from the initial position. (b) Reach the lesion site. (c) Switch to the targeted therapeutic delivery mode. (d) The targeted therapeutic delivery mode. (e) Treat the lesion site. (f) Move forward to end position.

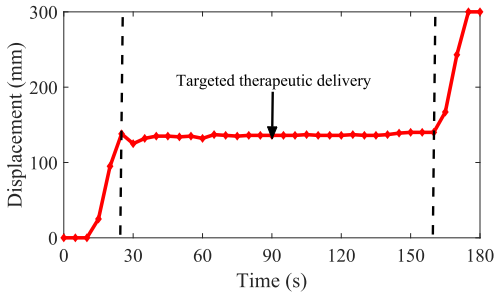

Fig. 11. Displacement of ATTDM for targeted therapeutic delivery.

C. Ex Vivo Experiments of ATTDM

Ex vivo experiments are carried out on a fresh porcine intestine filled with water to evaluate the motion characteristics of ATTDM, as shown in Fig. 9(a). The maximum motion velocity of ATTDM in porcine intestine is 6.77 mm/s, which is lower than the maximum motion velocity in pipe of 32.47 mm/s. This is because the random growth of many fat particles inside porcine intestine hinders the normal rotation of the spiral structure. Ultimately, ATTDM is subject to extra resistance, resulting in a decrease in motion velocity.

Meanwhile, ATTDM prototype is used to mimicking the treatment in clinics and its position is photographed by the X-ray fluoroscopy system, as shown in Fig. 12. First, ATTDM rotates and moves forward in the porcine intestine, as shown in Fig. 12(a). When reaching the lesion site, ATTDM switches to the targeted therapeutic delivery mode, as shown in Fig. 12(b) and Fig. 12(c). Through the X-ray images, it can be clearly observed that ATTDM anchored at the lesion site. After the treatment, ATTDM excluded from the porcine intestinal tract, as shown in Fig. 12(d). This experiment verifies the feasibility that ATTDM can perform tasks such as movement, anchoring and targeted therapeutic delivery in a more complex environment.

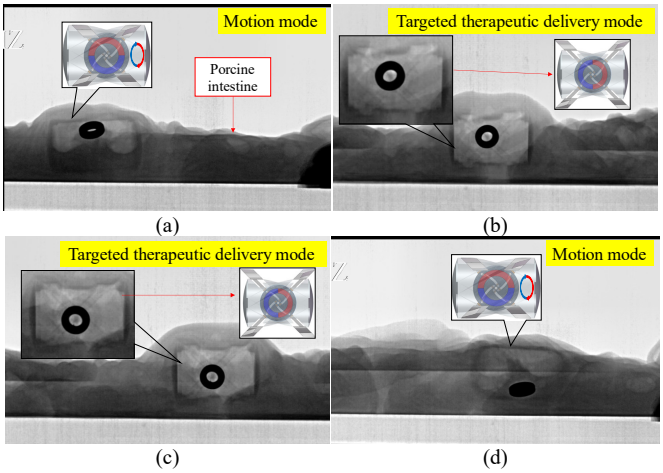

Fig. 12. Ex vivo experiments of ATTDM: (a) move forward, (b) switch to the targeted therapeutic delivery mode, (c) targeted therapeutic delivery, (d) excluded from the intestinal.

VI. Discussion

This paper focuses on the realization of the active movement and targeted drug delivery of ATTDM after anchoring through the targeted delivery mechanism. The prototype and corresponding experiments verify the function and feasibility of the proposed ATTDM. In clinical application, the X-ray fluoroscopy system can be used to provide position feedback for ATTDM, and the shell can be made of biocompatible material to meet the biocompatibility with human body.

The overall comparison between ATTDM and other similar drug delivery robots is provided in Table II. Although the design in [36] can realize drug delivery, there is a certain risk of leakage when using batteries as power supply. The design in [25] and [26] can only move to the lesion site, but cannot be fixed in the constantly peristaltic human intestine. Although the design in [37] can be anchored, its size is large and it lacks active motion mechanism. Based on the above comparison, the proposed ATTDM can not only move flexibly, but also targeted therapeutic delivery after being anchored in the constantly peristaltic intestine.

TABLE II
Comparison Between ATTDM and Previous Work

Work	Size (mm)	Power	Active motion	Anchoring
[36]	Φ10×35	Battery	--	--
[25]	Φ20×24	Magnetic	Yes	--
[26]	Φ18×30	Magnetic	Yes	--
[37]	Φ16×50	Magnetic	--	Yes
ATTDM	**Φ20×28**	**Magnetic**	**Yes**	**Yes**

VII. Conclusion

In this paper, the ATTDM is proposed to deliver drugs to the lesion site of the constantly peristaltic intestine through external magnetic field. It miniaturizes the targeted delivery mechanism and shows more effective functions than previous magnetic actuated microrobots. It can be converted into motion mode for flexible movement in the fluid environment, or into targeted therapeutic delivery mode for anchoring and targeted therapeutic delivery at the lesion site. Various dynamic models and simulations under different environments are established. Through the simulation and experimental results of ATTDM's motion, targeted therapeutic delivery and other different functions, the feasibility of controlling ATTDM with EPM is verified. From the experimental results, in the fluid filled tubular environment, the frequency and the motion velocity keep increasing linearly until reaching the cut-off frequency of ATTDM. Moreover, ATTDM can maintain flexible movement when confronted with various flow rate environments. The experimental results also prove that ATTDM can still complete targeted therapeutic delivery task with stable efficiency in the environment simulating intestinal peristalsis. Finally, through the experiment of fresh porcine intestine, it is well verified that ATTDM can anchor and targeted therapeutic delivery in the actual intestine.

Compared with the conventional capsule robots, ATTDM is superior in its movement and targeted delivery mechanism. It has improved the shortcomings of multiple permanent magnets to achieve multiple functions, as well as the limitation of being unable to anchor and deliver drugs in the constantly peristaltic intestine. In the future, we will further study the precise dose of targeted therapeutic delivery of ATTDM, treat specific clinical diseases, and conduct further research in the real environment of living animals.

References

[1] G. Iddan, G. Meron, A. Glukhovsky, and P. Swain, "Wireless capsule endoscopy," *Nature*, vol. 405, no. 6785, pp. 417-418, 2000.

[2] Y. Wang, T. Nitta, Y. Hiratsuka, and K. Morishima, "In situ integrated microrobots driven by artificial muscles built from biomolecular motors," *Sci. Robot.*, vol. 7, no. 69, pp. 13, 2022.

[3] T. Wang, H. Ugurlu, Y. Yan, M. T. Li, M. Li, A. Wild, E. Yildiz, M. Schneider, D. Sheehan, W. Hu, and M. Sitti, "Adaptive wireless millirobotic locomotion into distal vasculature," *Nat. Commun.*, vol. 13, no. 1, pp. 17, 2022.

[4] T. Xu, C. Huang, Z. Lai, and X. Wu, "Independent control strategy of multiple magnetic flexible millirobots for position control and path following," *IEEE Trans. Robot.*, vol. 38, no. 5, pp. 2875-2887, 2022.

[5] T. Xu, Z. Hao, C. Huang, J. Yu, L. Zhang, and X. Wu, "Multimodal locomotion control of needle-like microrobots assembled by ferromagnetic nanoparticles," *IEEE ASME Trans Mechatron*, vol. 27, no. 6, pp. 4327-4338, 2022.

[6] S. Xu, J. Liu, C. Yang, X. Wu, and T. Xu, "A learning-based stable servo control strategy using broad learning system applied for microrobotic control," *IEEE Trans Cybern*, vol. 52, no. 12, pp. 13727-13737, 2021.

[7] B. Zhang and Y. H., "The mechanism of action of microrobots in tumor treatment," *Int. J. Oncol.*, vol. 47, no. 10, pp. 624-626, 2020.

[8] S. Hwang, A. Ramos-Sebastian, and S. H. Kim, "Feedbackless automatic control of magnetic milli/microrobots: Generation and control of a trapping point using a single coil electromagnetic system," *IEEE ASME Trans Mechatron*, vol. 27, no. 5, pp. 2997-3007, 2022.

[9] F. Liu, X. Liu, Q. Huang, and T. Arai, "Recent progress of magnetically actuated DNA micro/nanorobots," *Cyborg Bionic Syst.*, vol. 2022, pp. 9758460, 2022.

[10] J. Guo, Z. Bao, Q. Fu, and S. Guo, "Design and implementation of a novel wireless modular capsule robotic system in pipe," *Med. Biol. Eng. Comput.*, vol. 58, no. 10, pp. 2305-2324, 2020.

[11] J. Li, L. Dekanovsky, B. Khezri, B. Wu, H. Zhou, and Z. Sofer, "Biohybrid micro- and nanorobots for intelligent drug delivery," *Cyborg Bionic Syst.*, vol. 2022, pp. 9824057, 2022.

[12] G. Pittiglio, L. Barducci, J. W. Martin, J. C. Norton, C. A. Avizzano, K. L. Obstein, and P. Valdastri, "Magnetic levitation for soft-tethered capsule colonoscopy actuated with a single permanent magnet: A dynamic control approach," *IEEE Robot. Autom. Lett.*, vol. 4, no. 2, pp. 1224-1231, 2019.

[13] P. Valdastri, R. J. Webster, C. Quaglia, M. Quirini, A. Menciassi, and P. Dario, "A new mechanism for mesoscale legged locomotion in compliant tubular environments," *IEEE Trans. Robot.*, vol. 25, no. 5, pp. 1047-1057, 2009.

[14] M. Su, T. Xu, Z. Lai, C. Huang, J. Liu, and X. Wu, "Double-modal locomotion and application of soft cruciform thin-film microrobot," *IEEE Robot. Autom. Lett.*, vol. 5, no. 2, pp. 806-812, 2020.

[15] D. Liu, X. Liu, Z. Chen, Z. Zuo, X. Tang, Q. Huang, and T. Arai, "Magnetically driven soft continuum microrobot for intravascular operations in microscale," *Cyborg Bionic Syst.*, vol. 2022, pp. 9850832, 2022.

[16] X. Pi, Y. Lin, K. Wei, H. Liu, G. Wang, X. Zheng, Z. Wen, and D. Li, "A novel micro-fabricated thruster for drug release in remote controlled capsule," *Sens. Actuator A Phys.*, vol. 159, no. 2, pp. 227-232, 2010.

[17] C. Dietzel, H. Richert, S. Abert, U. Merkel, M. Hippius, and A. Stallmach, "Magnetic active agent release system (MAARS): Evaluation of a new way for a reproducible, externally controlled drug release into the small intestine," *J. Control. Release*, vol. 161, no. 3, pp. 722-727, 2012.

[18] M. Beccani, C. Di Natali, G. Aiello, C. Benjamin, E. Susilo, and P. Valdastri, "A magnetic drug delivery capsule based on a coil actuation mechanism," *Procedia Eng.*, vol. 120, pp. 53-56, 2015.

[19] M. Simi, P. Valdastri, C. Quaglia, A. Menciassi, and P. Dario, "Design, fabrication, and testing of a capsule with hybrid locomotion for gastrointestinal tract exploration," *IEEE ASME Trans Mechatron*, vol. 15, no. 2, pp. 170-180, 2010.

[20] Z. Yang, L. Yang, and L. Zhang, "Autonomous navigation of magnetic microrobots in a large workspace using mobile-coil system," *IEEE ASME Trans Mechatron*, vol. 26, no. 6, pp. 3163-3174, 2021.

[21] J. Lu, Y. Liu, W. Huang, K. Bi, Y. Zhu, and Q. Fan, "Robust control strategy of gradient magnetic drive for microrobots based on extended state observer," *Cyborg Bionic Syst.*, vol. 2022, pp. 9835014, 2022.

[22] L. Manfredi, E. Capoccia, G. Ciuti, and A. Cuschieri, "A soft pneumatic inchworm double balloon (SPID) for colonoscopy," *Sci. Rep.*, vol. 9, pp. 9, 2019.

[23] Q. Fu, S. X. Guo, Y. Yamauchi, H. Hirata, and H. Ishihara, "A novel hybrid microrobot using rotational magnetic field for medical applications," *Biomed. Microdevices*, vol. 17, no. 2, pp. 12, 2015.

[24] V. Le, H. Rodriguez, C. Lee, G. Go, J. Zhen, V. Du Nguyen, H. Choi, S. Ko, J. Park, and S. Park, "A soft-magnet-based drug-delivery module for active locomotive intestinal capsule endoscopy using an electromagnetic actuation system," *Sens. Actuator A Phys.*, vol. 243, pp. 81-89, 2016.

[25] Z. Wang, S. Guo, J. Guo, Q. Fu, L. Zheng, and T. Tamiya, "Selective motion control of a novel magnetic-driven minirobot with targeted drug sustained-release function," *IEEE ASME Trans Mechatron*, vol. 27, no. 1, pp. 336-347, 2022.

[26] Z. Cai, Q. Fu, S. Zhang, C. Fan, X. Zhang, J. Guo, and S. Guo, "Performance evaluation of a magnetically driven microrobot for targeted drug delivery," *Micromachines*, vol. 12, no. 10, pp. 18, 2021.

[27] S. Tasoglu, E. Diller, S. Guven, M. Sitti, and U. Demirci, "Untethered micro-robotic coding of three-dimensional material composition," *Nat. Commun.*, vol. 5, pp. 9, 2014.

[28] J. Zhang, Y. Liu, J. Tian, D. Zhu, and S. Prasad, "Design and experimental investigation of a vibro-impact capsule robot for colonoscopy," *IEEE Robot. Autom. Lett.*, vol. 8, no. 3, pp. 1842-1849, 2023.

[29] Q. Fu, C. Fan, X. Wang, S. Zhang, X. Zhang, J. Guo, and S. Guo, "A compensation method for magnetic localization on capsule robot in medical application," *IEEE Sens. J.*, vol. 21, no. 23, pp. 26690-26698, 2021.

[30] J. J. Abbott, K. E. Peyer, M. C. Lagomarsino, L. Zhang, L. X. Dong, I. K. Kaliakatsos, and B. J. Nelson, "How should microrobots swim?," *Int. J. Robot. Res.*, vol. 28, no. 11-12, pp. 1434-1447, 2009.

[31] B. Ye, Z. Q. Zhong, W. Zhang, and D. H. Hu, "Research on coaxial control of magnetic spiral-type capsule endoscope," *IEEE Access*, vol. 8, pp. 108113-108120, 2020.

[32] Y. Kim and X. H. Zhao, "Magnetic soft materials and robots," *Chem. Rev.*, vol. 122, no. 5, pp. 5317-5364, 2022.

[33] A. W. Mahoney and J. J. Abbott, "Five-degree-of-freedom manipulation of an untethered magnetic device in fluid using a single permanent magnet with application in stomach capsule endoscopy," *Int. J. Robot. Res.*, vol. 35, no. 1-3, pp. 129-147, 2016.

[34] Z. Cai, Q. Fu, S. Zhang, S. Guo, J. Guo, X. Zhang, and C. Fan, "Characteristic analysis of a magnetically actuated capsule microrobot in medical applications," *IEEE Trans. Instrum. Meas.*, vol. 71, pp. 11, 2022.

[35] K. Arce, S. Waris, A. E. Alexander, and K. S. Ettinger, "Novel patient-specific 3-dimensional printed fixation tray for mandibular reconstruction with fibular free flaps," *J. Oral Maxillofac. Surg.*, vol. 76, no. 10, pp. 2211-2219, 2018.

[36] M. E. A. McGirr, S. M. McAllister, E. E. Peters, A. W. Vickers, A. R. Parr, and A. W. Basit, "The use of the InteliSite (R) companion device to deliver mucoadhesive polymers to the dog colon," *Eur. J. Pharm. Sci.*, vol. 36, no. 4-5, pp. 386-391, 2009.

[37] S. Song, S. Yuan, F. Zhang, J. Su, D. Ye, J. Wang, and M. Q. Meng, "Integrated design and decoupled control of anchoring and drug release for wireless capsule robots," *IEEE ASME Trans Mechatron*, vol. 27, no. 5, pp. 2897-2907, 2022.